Available online at website: https://journal.bcrec.id/index.php/bcrec

Bulletin of Chemical Reaction Engineering & Catalysis, 19 (2) 2024, 181-189

Research Article

Efficient Adsorption of Methylene Blue Dye Using Ni/Al Layered Double Hydroxide-Graphene Oxide Composite

Amri Amri[1], Sahrul Wibiyan[1], Alfan Wijaya[1], Nur Ahmad[1], Risfidian Mohadi[2], Aldes Lesbani[1,2,*]

[1]Research Center of Inorganic Materials and Coordination Complexes, Faculty of Mathematics and Natural Sciences, Universitas Sriwijaya, Palembang, 30139, Indonesia.
[2]Master Program of Material Science, Graduate School Universitas Sriwijaya, Palembang, 30139, Indonesia.

Received: 19th January 2024; Revised: 18th February 2024; Accepted: 21st February 2024
Available online: 5th March 2024; Published regularly: August 2024

Abstract

To address environmental pollution, we developed Ni/Al layered double hydroxide-graphene oxide (Ni/Al-GO) adsorbent materials for the purpose of eliminating methylene blue (MB) dye pollutants. The adsorption process was explored by examining many experimental factors, including temperature, regeneration/reuse procedure, pH, and time, and their effects on the material. The appropriate model for the isotherm is the Langmuir isotherm. The Ni/Al-GO material achieved a maximum adsorption capacity of 61.35 mg/g for MB dye at a temperature of 60 °C. The thermodynamic characteristics indicate that the adsorption process is both endothermic and spontaneous as the temperature increases. The regeneration method demonstrated that the Ni/Al-GO material has a highly stable structure, enabling it to be utilized for five cycles with a remarkable regeneration rate of 93.49% in the fifth cycle. The pH that yielded the best results for all materials was pH 10, and the kinetic model demonstrated a pseudo second-order behavior.

Keywords: Layered double hydroxide; Graphene Oxide; Methylene Blue; Adsorption

How to Cite: A. Amri, S. Wibiyan, A. Wijaya, N. Ahmad, R. Mohadi, A. Lesbani (2024). Efficient Adsorption of Methylene Blue Dye Using Ni/Al Layered Double Hydroxide-Graphene Oxide Composite. *Bulletin of Chemical Reaction Engineering & Catalysis*, 19 (2), 181-189 (doi: 10.9767/bcrec.20121)

Permalink/DOI: https://doi.org/10.9767/bcrec.20121

1. Introduction

Water is a highly precious resource on Earth. Water is extensively utilised as a primary catalyst in the process of growth and industry [1]. In recent years, the growing industrialization activities have caused serious environmental pollution [2]. One of the industrialization activities that cause environmental pollution is dyes, which are the main raw materials in the textile and paper industry [3].

Methylene blue (MB) is a cationic dye that is commonly used to color wool and cotton in the textile and paper industries [4]. It is known that MB is very harmful to human health because it can cause vomiting, shock, diarrhea, increased heart rate, tissue damage and carcinogenic causes [5,6]. Various methods can be used in removing MB dye pollutants, including coagulation, flocculation, membrane filtration, advanced oxidation process, photocatalytic degradation, and adsorption [7–11]. Adsorption is the most extensively utilized approach among these options due to its ease of use, low cost, and high efficacy [12–14].

Layered double hydroxide (LDH) is an aninoic layered compound consisting of metal charges (M^{2+} and M^{3+}), hydroxyl groups, and interlamellar anions [15]. In particular, LDH has been widely used in MB dye removal process due to its outstanding ion exchange and adsorption ability [16]. However, LDH has the disadvantage of poor structural stability, which makes the efficiency of material reuse/recession unfavorable due to easy peeling of the structure during application [17]. Hence, it is imperative to enhance the composition by using carbon components. Ahmad *et al.* [18] enhanced the configuration of LDH by including

* Corresponding Author.
Email: aldeslesbani@pps.unsri.ac.id (A. Lesbani)

magnetic humic acid, resulting in better structural stability and increased adsorption capacity. This was achieved by introducing functional sites into the material, allowing for regeneration up to five times. It can be seen that in the fifth cycle, LDH composited with humic acid magnetic has a percentage of adsorption ability of >90% compared to LDH alone which has a percentage of adsorption ability of only 21%.

Graphene oxide (GO) is a monolayer material with a planar structure that arises from the oxidation process of graphite. Graphene oxide (GO) possesses a substantial surface area and many oxygen functional groups, including carboxyl (−COOH), hydroxyl (−OH), epoxy (−O−), and carbonyl (−C=O). These characteristics render GO highly effective in eliminating water contaminants [19].

In this study, layered double hydroxide structure modification was carried out by compositing graphene oxide to improve the structure stability and adsorption capacity of MB dye. Layered double hydroxide Ni/Al-graphene oxide was synthesized and XRD, FT-IR, and BET characterization were carried out to identify the success of material preparation. In addition, MB dye is treated on the material through several variations, including the effect of temperature and concentration (adsorption isotherms and thermodynamics), regeneration processes that assess structural stability, pH, and time (kinetics).

2. Materials and Methods

2.1 Chemicals and Instrumentation

The materials used in this study include distilled water (H_2O), graphite and methylene blue dye ($C_{16}H_{18}ClN_3S$). In addition, there are also chemicals, such as sulfuric acid (H_2SO_4) and hydrochloric acid (HCl) obtained from LabGuard®. The compounds aluminium nitrate nonahydrate ($Al(NO_3)_3.9H_2O$), sodium chloride (NaCl), nickel nitrate hexahydrate ($Ni(NO_3)_2.6H_2O$), sodium hydroxide (NaOH), and sodium carbonate (Na_2CO_3) were acquired from SigmaAldrich. The research utilised the following instruments for support: a Rigaku Miniflex-6000 X-Ray Diffraction (XRD) instrument, a NOVA 4200e Surface Area & Pore Size Analyzer (BET) instrument, a Shimadzu Prestige-21 Fourier Transform Infra-Red (FTIR) instrument, and a Biobase BK-UV 1800 PC UV-Vis spectrophotometer set at a wavelength of 664 nm.

2.2 Synthesis of NiAl LDH

The synthesis of Ni/Al LDH was achieved using a co-precipitation method. A solution of 100 mL of 0.75 M $Ni(NO_3)_2.6H_2O$ and 0.25 M $Al(NO_3)_3.9H_2O$ was prepared in a Becker beaker. In addition, the solution was gradually added with a combination of 50 mL 2 M NaOH and 100 mL 2 M Na_2CO_3. Subsequently, a 2 M NaOH solution was added to the solution in order to achieve a pH of 10. The solution was agitated for a duration of 17 h at a temperature of 80 °C. Following the formation of the precipitate, it underwent filtration, drying, and characterization using XRD, FT-IR, and BET analysis.

2.3 Preparation of Ni/Al-GO

The composite material was fabricated by the co-precipitation technique by combining a solution of Ni/Al LDH with graphene oxide material generated using the Hummer process [20]. Subsequently, a total of 30 mL of the solutions $Ni(NO_3)_2.6H_2O$ 0.75 M and $Al(NO_3)_3.9H_2O$ 0.25 M were mixed together. The mixture was gradually infused with a solution composed of 15 mL of 2 M NaOH and 30 mL of 2 M Na_2CO_3. Subsequently, a 2 M NaOH solution was introduced into the combined solution in order to adjust its pH to 10. Subsequently, the solution was agitated for a duration of 1 h, following which 3 g of graphene oxide were introduced. The heterogeneous solution was agitated for a duration of 72 h at a temperature of 80 °C. The resulting solid was further filtered, desiccated, and subjected to analysis using X-ray diffraction (XRD), Fourier-transform infrared spectroscopy (FT-IR), and Brunauer-Emmett-Teller (BET) surface area measurement.

2.4 Determination of PZC on Each Adsorbent

Determination of PZC is done to determine the state of the material/adsorbent in an uncharged state. This procedure involves preparing a 20 mL 0.1 M NaCl solution that has been adjusted to pH 2-11 using HCl and NaOH. The NaCl solution that has been prepared is then added 0.02 g of adsorbent and stirred for 24 h. After the stirring process is complete, the pH is then measured again to see the final pH. The data obtained, then plotted between the initial pH and the difference between the final pH and the initial pH (ΔpH).

2.5 Adsorption of Methylene Blue Dye

The effect of concentration and temperature (adsorption isotherms and thermodynamics), adsorbent regeneration/reuse process, pH, time (adsorption kinetics) are some of the parameters examined during the methylene blue dye adsorption process. The investigation process was carried out by mixing 20 mL of methylene blue dye solution with 0.02 g of adsorbent. This study investigated the relationship between

concentration and temperature using concentrations of 15, 25, 35, 45, and 55 mg/L (30-60 °C) and the adsorbent reuse/regeneration process was performed in five cycles. The effect of pH was done by setting the pH from pH 2-10. The effect of time was done by setting the time from 0, 10, 20, 30, 45, 60, 75, 90, and 120 min.

2.6 Desorption and Regeneration Process of Adsorbent in Methylene Blue Adsorption

Desorption is the process of releasing the adsorbate from the adsorbent. The desorption procedure began with an initial adsorption process including 20 mL of MB and 0.02 g of adsorbent. The mixture was agitated for 2 h before being tested. The filtrate was tested to determine the adsorbed concentration. The leftover adsorbent collected as a precipitate was dried and desorbed using 10 mL of distilled water with the assistance of an ultrasonic instrument. The regeneration procedure involved repeating the adsorption and desorption process up to five times.

3. Results and Discussion

3.1 Characterization of the Adsorbent Materials

The XRD patterns of Ni/Al LDH and NiAl-GO materials can be seen in Figure 1. The Ni/Al LDH material shows diffraction peaks at 2θ angles of 11.81°, 23.16°, 35.32°, 39.01°, 61°, and 62.48° which correspond to (003), (006), (012), (015), (110), and (113) which are characteristic of the crystal plane of Ni/Al LDH (JCPDS NO.15-0087) [21,22]. After the addition of graphene oxide to the Ni/Al LDH material, it can be seen that the crystallinity structure of Ni/Al is weakened. This can be seen in the Ni/Al-GO structure in the (003) and (006) crystal planes experiencing a decrease in intensity and peak broadening [23,24]. According to Rashed *et al.* [25], the addition of carbon material, namely graphene oxide, to LDH can result in a shift in the peak in the crystal plane (003) towards a lower 2θ angle. It can be seen that the diffraction peak at 2θ angle 11.81° in LDH has shifted to 11.6° after the addition of graphene oxide material.

The Fourier transform infrared (FTIR) spectra of the Ni/Al-GO and Ni/Al LDH materials are displayed in Figure 2. The broad peaks at 3449 cm^{-1} and 1620 cm^{-1} are due to the bending vibrations of water molecules. The vibrations of NO_3^- are responsible for the peak at 1381 cm^{-1}. This suggests that the interlayer gap added in LDH contains nitrate anion [26]. The stretching of M−O−H and M−O (M = Ni and Al) is shown by the peaks at 602 cm^{-1} and 563 cm^{-1} [26,27]. In the Ni/Al-GO material, it can be seen that there is a peak at 3410 cm^{-1} indicating the −OH stretching vibration of hydroxyl and carboxyl. The carbonyl and carboxylic groups' C=O stretching vibrations are shown by the peak at 1720 cm^{-1}. C=C stretch vibrations are present by the peak at 1589 cm^{-1}. The C−O−C stretching vibrations of the epoxy group and the C−O stretching vibrations of the hydroxyl surface are shown by the peaks at 1242 and 1103 cm^{-1}, respectively [19]. In addition to displaying typical peaks of GO materials, Ni/Al-GO materials still have peaks from LDH, namely having NO_3^- anions marked at 1381 cm^{-1} and stretching vibrations from M−O−H and M−O at 617 and 578 cm^{-1}.

N_2 adsorption-desorption isotherms on Ni/Al LDH and Ni/Al-GO materials can be seen in Figure 3. Based on the IUPAC classification, both materials show type IV hysteresis loop isotherms which indicate mesoporous materials (2-50 nm) [28]. Table 1 presents the results of N_2 adsorption-

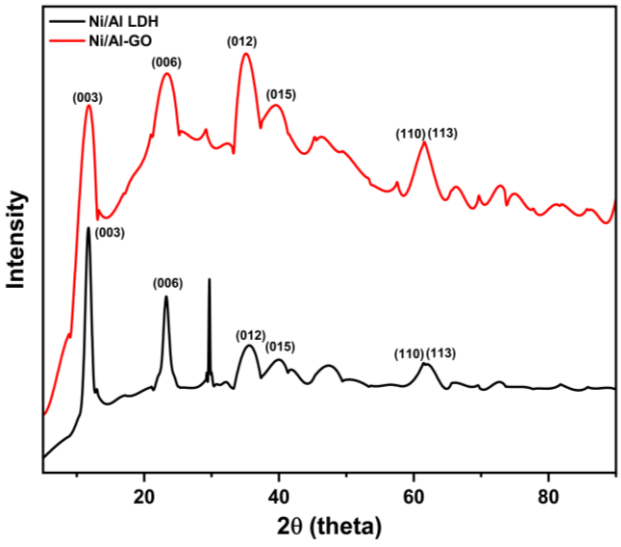

Figure 1. X-Ray diffractogram of adsorbents.

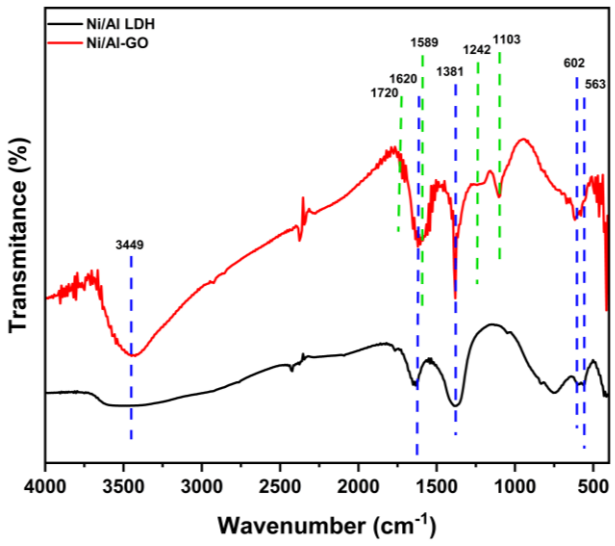

Figure 2. Fourier transfer infra-red spectrum of adsorbents.

desorption isotherms, which include specific surface area, pore size distribution, and pore volume. The specific surface area of a material is a crucial component that directly influences the efficacy of its adsorption process. The results indicate that the surface area of the Ni/Al-GO material is twice as large as that of the Ni/Al LDH material. The incorporation of graphene oxide (GO) into the Ni/Al layered double hydroxide (LDH) material resulted in an increase in surface area. The surface area of Ni/Al-GO material is 78.35 m^2/g, which is higher than the surface area of Ni/Al LDH material, which is 40.91 m^2/g. The pore size distribution shows that both materials are porous with mesoporous holes whose diameter range is 2-8 nm.

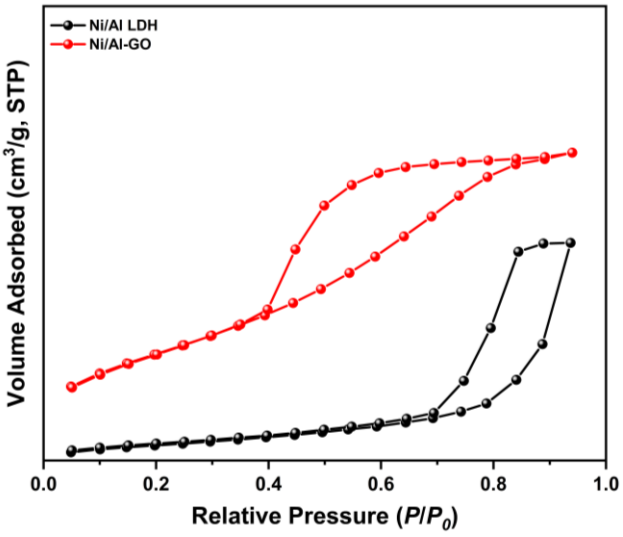

Figure 3. N_2 adsorption-desorption isotherms of adsorbents.

3.2 Effect of Isotherms and Thermodynamic Studies

Table 2 presents the use of Langmuir and Freundlich isotherm models to analyse the experimental findings and understand the adsorption interactions occurring on MB dye. According to the collected data, both materials have a tendency to conform to the Langmuir isotherm model. The R^2 value in the Langmuir

Table 1. Brunauer-Emmet-Teller Surface Area, Pore Size and Pore Volume of adsorbents.

Material	Surface Area (m^2/g)	Pore Size (nm), BJH	Pore Volume (cm^3/g), BJH
Ni/Al LDH	40.91	7.46	0.153
Ni/Al-GO	78.35	2.41	0.095

Tabel 2. Langmuir and Freundlich parameter.

Adsorbent	T (°C)	Langmuir			Freundlich		
		Q_{max}	k_L	R^2	n	k_F	R^2
Ni/Al LDH	30	29.326	0.020	0.545	1.332	0.876	0.823
	40	42.017	0.022	0.702	1.347	1.369	0.897
	50	35.971	0.055	0.820	1.686	3.145	0.786
	60	31.847	0.163	0.977	2.487	7.333	0.826
Ni/Al-GO	30	60.976	0.698	0.572	29.586	30.946	0.007
	40	61.350	1.156	0.750	22.523	32.144	0.016
	50	59.172	1.899	0.902	8.210	34.419	0.114
	60	54.945	9.100	0.996	7.728	40.142	0.225

Table 3. Comparison of the Q_{max} of several adsorbents with Ni/Al LDH and Ni/Al-GO materials that have been published in the literatures.

Adsorbent	Q_{max} (mg/g)	Reference
Bagasse Fly Ash	15.5	[30]
orange lemon peel activated carbon	38	[31]
Three-dimensional MgAl LDH	58.3	[32]
Hydroxyapatite	38.93	[33]
Natural clay	50.25	[34]
starch/poly(acylic acid) hydrogels	26.7	[35]
Raw pine leaf biomass	36.88	[36]
g-C_3N_4@NiCo LDH	25.06	[37]
Magnetic rhamnolipid-Co/Al LDH	54.01	[38]
Zn-Co-Fe/LDH	58.26	[39]
Ni/Al LDH	42.017	This study
Ni/Al-GO	61.350	This study

isotherm model exceeds the R^2 value in the Freundlich isotherm model. The Langmuir isotherm model explains the homogenous process of adsorption, where adsorbate molecules form a monolayer on the surface of the adsorbent. This model is described in reference [29]. The greatest adsorption capacities for Ni/Al LDH and Ni/Al-GO were 42.017 mg/g and 61.350 mg/g, respectively. Table 3 presents a juxtaposition of the highest adsorption capacity values of various materials in relation to other materials.

The adsorption thermodynamic parameters such as ΔH, ΔS, and ΔG are shown in Table 4. The calculation of the thermodynamic parameters ΔH and ΔS was performed by utilizing the Van't Hoff equation (Equation (1)), whereas the calculation of ΔG was undertaken by utilizing Equation (2):

$$\ln \frac{q_e}{C_e} = \frac{\Delta S}{R} - \frac{\Delta H}{RT} \quad (1)$$

$$\Delta G = \Delta H - T\Delta S \quad (2)$$

where, q_e represents equilibrium adsorption capacity in milligrams per gram, C_e is the equilibrium dye concentration in milligrams per liter, R is the universal gas constant, T stands for temperature in Kelvin, ΔS denotes entropy, ΔG represents Gibbs free energy, and ΔH symbolizes enthalpy.

The results obtained show a positive ΔH which indicates the adsorption process is endothermic. The small ΔS indicates the low value of degrees of freedom. ΔG obtained shows that as the temperature increases, the resulting value is increasingly negative. This shows that the adsorption process at high temperatures makes the adsorption process easier.

3.3 Regeneration of Adsorbents

The effectiveness of the adsorbent in the regeneration process can be seen in Figure 4. Figure 4 shows that the Ni/Al-GO material has a very good regeneration percentage. The first cycle had a regeneration percentage of 97.37%, which gradually decreased to 93.49% by the fifth cycle, showing a negligible decline. Unlike the Ni/Al LDH material, which has a low regeneration percentage, it also underwent a substantial decline from 45.27% to 1.85% by the fifth cycle. These findings suggest that the incorporation of GO material into the LDH material enhances the structural stability of the Ni/Al-GO material.

3.4 Effect of Point Zero Charge (PZC) Materials and pH Effect on MB Dye Adsorption

The pzc value is utilised to determine the condition of a substance while it is in a neutral state. The PZC value is determined by graphing the discrepancy between the final pH and the beginning pH (ΔpH), as seen in Figure 5(a). The obtained results indicate that the Ni/Al LDH and Ni/Al-GO materials possess point of zero charge (PZC) values of 7.4 and 6.8, respectively. When the pH is lower than the point of zero charge (PZC), the material's surface has a positive charge. In contrast, if the pH is higher than the point of zero charge (PZC), the material's surface has a negative charge. Consequently, it can be inferred that the anticipated pH level is higher

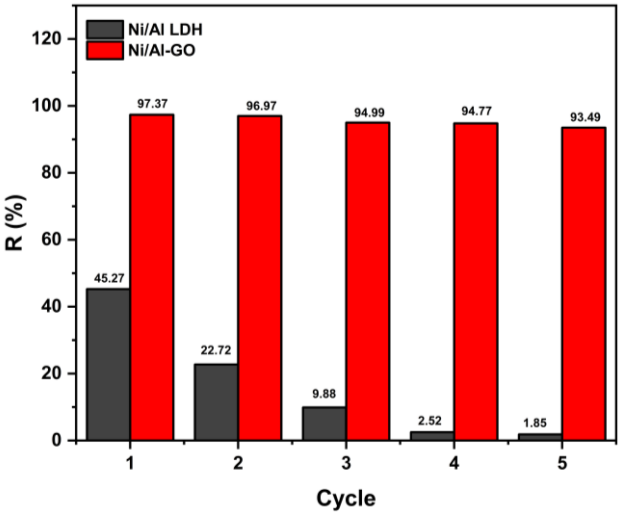

Figure 4. Regeneration of Ni/Al LDH and Ni/Al-GO.

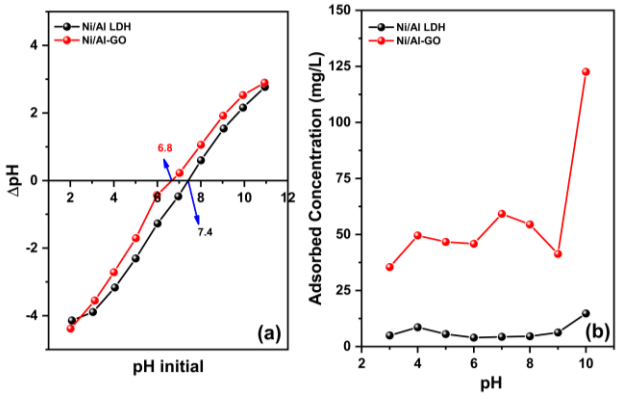

Figure 5. Point Zero Charge (PZC) of adsrobents (a) and Effect of pH on MB adsorption (b).

Table 4. Adsorption thermodynamic parameter.

Adsorbent	Concentration (mg/L)	ΔH (kJ/mol)	ΔS (kJ/mol)	ΔG (kJ/mol)			
				303 K	313 K	323 K	333 K
Ni/Al LDH	35	40.076	0.126	1.815	0.553	−0.710	−1.973
Ni/Al-GO	35	32.431	0.153	−13.891	−15.420	−16.948	−18.477

than the point of zero charge (PZC), enabling the material to absorb MB dye through the influence of electrostatic forces.

As demonstrated in Figure 5(b), the ideal pH for MB dye adsorption for each material is 10. The attraction between the positively charged MB dye and the negatively charged material surface is due to electrostatic forces. When the pH is below the point of zero charge (PZC), the surface of the material becomes positively charged, leading to a decrease in its adsorption capacity. The electrostatic repulsion force between the positively charged MB dye and the positively charged material surface is the underlying reason for this phenomenon.

3.5 Effect of Time and Kinetics study

Figure 6 illustrates the impact of contact time on the adsorption of MB dye on each adsorbent. As the duration of adsorption rises, the amount of adsorbed material also increases. The adsorption process exhibited a fast initial adsorption followed by a progressive decline till reaching equilibrium. The quick adsorption process is attributed to the many active sites on the surface of the adsorbent, which diminishes as equilibrium is approached.

A suitable kinetic model for the adsorption process of MB dye was determined using the pseudo first-order and pseudo second-order kinetic models, as specified in Table 5. Table 5 shows that the pseudo second-order kinetic model is more suitable than the pseudo first-order kinetic model. This is because the R^2 value of the pseudo second-order kinetic model is higher than the R^2 value of the pseudo first-order kinetic model. In addition, when comparing the Qe_{calc} value of the pseudo first-order kinetic model with the Qe_{calc} value of the pseudo second-order kinetic model, the Qe_{calc} value of the pseudo second-order kinetic model is closer to the Qe_{exp} value. Therefore, it can be concluded that the main process used to adsorb MB dye is chemisorption [40].

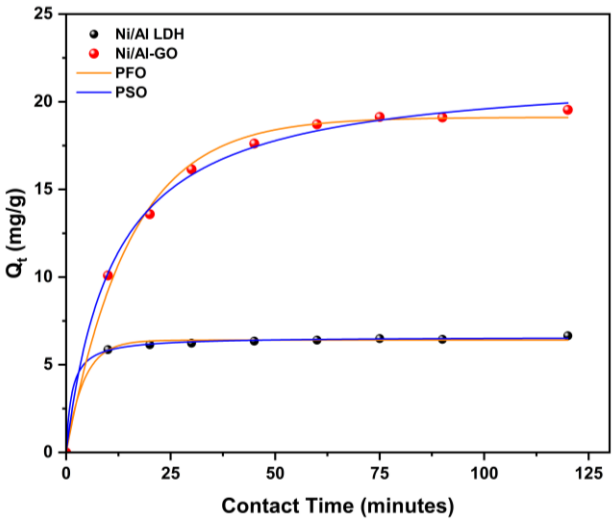

Figure 6. PFO and PSO kinetics models of adsorbents.

4. Conclusion

The synthesis of Ni/Al LDH and Ni/Al-GO materials was effectively achieved, as confirmed by the characterisation findings obtained from XRD, FT-IR, and BET analysis. The suitable model for adsorption is the Langmuir isotherm model. The Ni/Al-GO exhibited a higher maximum adsorption capacity compared to Ni/Al LDH, with values of 61.35 mg/g and 42.017 mg/g, respectively. The adsorption process exhibited an endothermic nature, and with increasing temperature, the adsorption process happened spontaneously. The regeneration process demonstrates the superior structural stability of the Ni/Al-GO material compared to the Ni/Al LDH material. The PZC (Point of Zero Charge) value of each material is 7.4 on Ni/Al LDH and 6.8 on Ni/Al-GO. Every substance has an ideal pH level of 10. The PSO model has been validated as the kinetics model.

Acknowledgement

In order to complete this research procedure, the author would like to thank the Research Center for Inorganic Materials and Coordination Complex, Sriwijaya University for the assistance and instrumentation analysis that has been provided.

CRediT Author Statement

Author Contributions: *A. Amri*: Conceptualization, Investigation, Writing-Original draft, Software, Visualization; *S. Wibiyan*: Formal analysis, Resources; *A. Wijaya*: Formal analysis, Visualization; *N. Ahmad*: Visualization, Formal Analysis; *R. Mohadi*: Validation, Data Curation; *A. Lesbani*:

Table 5. Kinetic parameters pseudo first-order and pseudo second-order models.

Adsorbents	Qe_{exp} (mg/g)	*Pseudo first-order*			*Pseudo second-order*		
		Qe_{calc} (mg/g)	k_1 (min^{-1})	R^2	Qe_{calc} (mg/g)	k_2 ($g.mg^{-1}.min^{-1}$)	R^2
Ni/Al LDH	6.655	4.130	0.061	0.720	6.698	0.0701	0.9995
Ni/Al-GO	19.542	40.992	0.078	0.801	21.413	0.005	0.9991

Methodology, Conceptualization, Funding acquisition, Resources, Writing-review & editing, Supervision. All authors have read and agreed to the published version of the manuscript.

References

[1] Valentini, F., Cerza, E., Campana, F., Marrocchi, A., Vaccaro, L. (2023). Efficient synthesis and investigation of waste-derived adsorbent for water purification. Exploring the impact of surface functionalization on methylene blue dye removal. *Bioresource Technology*, 390, 129847. DOI: 10.1016/j.biortech.2023.129847.

[2] Li, S., Li, X., Li, S., Xu, P., Liu, Z., Yu, S. (2023). In-situ preparation of lignin/Fe_3O_4 magnetic spheres as bifunctional material for the efficient removal of metal ions and methylene blue. *International Journal of Biological Macromolecules*, 259 (P2), 128971. DOI: 10.1016/j.ijbiomac.2023.128971.

[3] Oladipo, A.C., Aderibigbe, A.D., Olayemi, V.T., Ajibade, P.A., Clayton, H.S., Zolotarev, P.N., Clarkson, G.J., Walton, R.I., Tella, A.C. (2024). Photocatalytic degradation of methylene blue using sunlight-powered coordination polymers constructed from a tetracarboxylate linker. *Journal of Photochemistry and Photobiology A: Chemistry*, 448, 115331. DOI: 10.1016/j.jphotochem.2023.115331.

[4] Sun, S.F., Wan, H.F., Zhao, X., Gao, C., Xiao, L.P., Sun, R.C. (2023). Facile construction of lignin-based network composite hydrogel for efficient adsorption of methylene blue from wastewater. *International Journal of Biological Macromolecules*, 253(P1), 126688. DOI: 10.1016/j.ijbiomac.2023.126688.

[5] Yang, P., Lu, Y., Zhang, H., Li, R., Hu, X., Shahab, A., Elnaggar, A.Y., Alrefaei, A.F., AlmutairiI, M.H., Ali, E. (2024). Effective removal of methylene blue and crystal violet by low-cost biomass derived from eucalyptus: Characterization, experiments, and mechanism investigation. *Environmental Technology and Innovation*, 33, 103459. DOI: 10.1016/j.eti.2023.103459.

[6] Srinivasan, R. (2023). A sustainable and cyclic metal organic framework-driven Fenton process for efficient removal of methylene blue. *Inorganic Chemistry Communications*, 156, 111209. DOI: 10.1016/j.inoche.2023.111209.

[7] Wang, L., Xue, G., Ye, T., Li, J., Liu, C., Liu, J., Ma, P. (2023). Zn-modified biochar preparation from solvent free in-situ pyrolysis and its removal of methylene blue. *Diamond and Related Materials*, 140(PA), 110438. DOI: 10.1016/j.diamond.2023.110438.

[8] Khooni, M.A.K., Ahmadzadeh, H., Davardoostmanesh, M. (2024). Magnetic graphene oxide/Mg-Al layered double hydroxide nanocomposite as an efficient adsorbent for removal of methylene blue: A study of equilibrium isotherms, kinetics, thermodynamic and reusability. *Materials Science and Engineering: B*, 300, 117123. DOI: 10.1016/j.mseb.2023.117123.

[9] Handayani, T., Emriadi, Deswati, Ramadhani, P., Zein, R. (2024). Modelling studies of methylene blue dye removal using activated corn husk waste: Isotherm, kinetic and thermodynamic evaluation. *South African Journal of Chemical Engineering*, 47, 15–27. DOI: 10.1016/j.sajce.2023.10.003.

[10] Hegazy, S., Abdelwahab, N.A., Ramadan, A.M., Mohamed, S.K. (2024). Magnetic Fe_3O_4-grafted cellulose/graphene oxide nanocomposite for methylene blue removal from aqueous solutions: Synthesis and characterization. *Next Materials*, 3, 100064. DOI: 10.1016/j.nxmate.2023.100064.

[11] Hingrajiya, R.D., Patel, M.P. (2023). Fe_3O_4 modified chitosan based co-polymeric magnetic composite hydrogel: Synthesis, characterization and evaluation for the removal of methylene blue from aqueous solutions. *International Journal of Biological Macromolecules*, 244, 125251. DOI: 10.1016/j.ijbiomac.2023.125251.

[12] Amri, A., Hanifah, Y. (2023). Synthesis of Graphene Oxide using Hummers Method as Adsorbent of Malachite Green Dye. *Indonesian Journal of Material Research*, 1(1), 29–34. DOI: 10.26554/ijmr.2023113.

[13] Palapa, N.R., Amri, A., Hanifah, Y. (2023). Potential Indonesian Rice Husk for Wastewater Treatment Agricultural Waste Preparation and Dye Removal Application. *Indonesian Journal of Environmental Management and Sustainability*, 7(4), 160–165. DOI: 10.26554/ijems.2023.7.4.160-165.

[14] Siregar, P.M.S.B.N., Wijaya, A., Amri, A., Nduru, J.P., Hidayati, N., Lesbani, A., Mohadi, R. (2022). Layered Double Hydroxide / C(C= Humic Acid ; Hydrochar) As Adsorbents of Cr(VI). *Science and Technology Indonesia*, 7(1), 41–48. DOI: 10.26554/sti.2022.7.1.41-48.

[15] Ahmad, N., Rohmatullaili, Wijaya, A., Lesbani, A. (2023). Magnetite Humic Acid-decorated MgAl Layered Double Hydroxide and Its Application in Procion Red Adsorption. *Colloids and Surfaces A: Physicochemical and Engineering Aspects*, 684, 133042. DOI: 10.1016/j.colsurfa.2023.133042.

[16] Wang, Q., Peng, Y., Chen, M., Xu, M., Ding, J., Yao, Q., Lu, S. (2024). Synthesis of layered double hydroxides from municipal solid waste incineration fly ash for heavy metal adsorption. *Science of The Total Environment*, 912, 169482. DOI: 10.1016/j.scitotenv.2023.169482.

[17] Amri, A., Rezonsi, R., Ahmad, N., Taher, T., Palapa, N.R., Mohadi, R., Lesbani, A. (2023). Biochar-Modified Layered Double Hydroxide for Highly Efficient on Phenol Adsorption. *Bulletin of Chemical Reaction Engineering and Catalysis*, 18(3), 460–472. DOI: 10.9767/bcrec.19898.

[18] Ahmad, N., Suryani Arsyad, F., Royani, I., Mega Syah Bahar Nur Siregar, P., Taher, T., Lesbani, A. (2023). High regeneration of ZnAl/NiAl-Magnetite humic acid for adsorption of Congo red from aqueous solution. *Inorganic Chemistry Communications*, 150, 110517. DOI: 10.1016/j.inoche.2023.110517.

[19] Heshami, M., Taheri, B. (2024). An experimental study on the adsorption behavior of gold glycinate complex on graphene oxide. *Hydrometallurgy*, 224, 106229. DOI: 10.1016/j.hydromet.2023.106229.

[20] Yang, W., Cao, M. (2022). Study on the Difference in Adsorption Performance of Graphene Oxide and Carboxylated Graphene Oxide for Cu(II), Pb(II) Respectively and Mechanism Analysis. *Diamond and Related Materials*, 129, 109332. DOI: 10.1016/j.diamond.2022.109332.

[21] Sun, Y., Yuan, Q., Dong, Y., Wang, Y., He, N., Wen, D. (2023). Resistive switching of two-dimensional NiAl-layered double hydroxides and memory logical functions. *Journal of Alloys and Compounds*, 933, 167745. DOI: 10.1016/j.jallcom.2022.167745.

[22] Wu, M., Li, W., Yang, W., Han, Q., Yao, J., Zhao, M., Lu, X. (2023). Reduced self-discharge of supercapacitors based on surfactant-functionalized NiAl layered double hydroxide. *Journal of Energy Storage*, 73(PB), 108965. DOI: 10.1016/j.est.2023.108965.

[23] Giri, B.S., Sonwani, R.K., Varjani, S., Chaurasia, D., Varadavenkatesan, T., Chaturvedi, P., Yadav, S., Katiyar, V., Singh, R.S., Pandey, A. (2022). Highly efficient bio-adsorption of Malachite green using Chinese Fan-Palm Biochar (Livistona chinensis). *Chemosphere*, 287, 132282. DOI: 10.1016/j.chemosphere.2021.132282.

[24] Zhang, S., Fan, S., Liang, T., Wei, J., Zhu, T., Shen, Y., Yu, Z., Zhu, H., Wang, S., Hou, Y. (2023). Sn and dual-oxygen-vacancy in the Z-scheme $Bi_2Sn_2O_7$/Sn/NiAl-layered double hydroxide heterojunction synergistically enhanced photocatalytic activity toward carbon dioxide reduction. *Journal of Colloid and Interface Science*, 652 (PB), 1126–1137. DOI: 10.1016/j.jcis.2023.08.145.

[25] Rashed, S.H., Abd-Elhamid, A.I., Abdalkarim, S.Y.H., El-Sayed, R.H., El-Bardan, A.A., Soliman, H.M.A., Nayl, A.A. (2022). Preparation and Characterization of Layered-Double Hydroxides Decorated on Graphene Oxide for Dye Removal from Aqueous Solution. *Journal of Materials Research and Technology*, 17, 2782–2795. DOI: 10.1016/j.jmrt.2022.02.040.

[26] Zhang, Y., Li, L., Du, C., Wan, G., Wei, Q., Zhou, X., Su, Y., Xu, Y., Wang, G. (2023). Controllable coating NiAl-layered double hydroxides on carbon nanofibers as anticorrosive microwave absorbers. *Journal of Materials Science and Technology*, 151, 109–118. DOI: 10.1016/j.jmst.2022.12.022.

[27] Xu, Y., Zhang, X., Liu, Y., Wei, Y., Lan, F., Wang, R., Yang, Y., Chen, J. (2023). Trace N-doped manganese dioxide cooperated with Ping-pong chrysanthemum-like NiAl-layered double hydroxide on cathode for improving bioelectrochemical performance of microbial fuel cell. *Bioresource Technology*, 381, 129139. DOI: 10.1016/j.biortech.2023.129139.

[28] Monjezi, R., Azadi, R., Hamoule, T. (2024). Design, synthesis, and characterization of thiol-decorated cross-linked graphene oxide framework for high-capacity Hg^{2+} ion adsorption. *Journal of Saudi Chemical Society*, 28(1), 101786. DOI: 10.1016/j.jscs.2023.101786.

[29] Guo, X., Wang, J. (2019). Comparison of linearization methods for modeling the Langmuir adsorption isotherm. *Journal of Molecular Liquids*, 296, 111850. DOI: 10.1016/j.molliq.2019.111850.

[30] Meskel, A.G., Mussa, M., Meshesha, B.T., Habtu, N.G., Naik, S.V.C.S., V, B.P. (2023). Malachite Green and Methylene Blue Dye Removal Using Modified Bagasse Fly Ash: Adsorption Optimization Studies. *Environmental Challenges*, 14, 100829. DOI: 10.1016/j.envc.2023.100829.

[31] Ramutshatsha-Makhwedzha, D., Mavhungu, A., Moropeng, M.L., Mbaya, R. (2022). Activated carbon derived from waste orange and lemon peels for the adsorption of methyl orange and methylene blue dyes from wastewater. *Heliyon*, 8 (8), e09930. DOI: 10.1016/j.heliyon.2022.e09930.

[32] Pan, X., Zhang, M., Liu, H., Ouyang, S., Ding, N., Zhang, P. (2020). Adsorption behavior and mechanism of acid orange 7 and methylene blue on self-assembled three-dimensional MgAl layered double hydroxide: Experimental and DFT investigation. *Applied Surface Science*, 522, 146370. DOI: 10.1016/j.apsusc.2020.146370.

[33] Aaddouz, M., Azzaoui, K., Akartasse, N., Mejdoubi, E., Hammouti, B., Taleb, M., Sabbahi, R., Alshahateet, S.F. (2023). Removal of methylene blue from aqueous solution by adsorption onto hydroxyapatite nanoparticles. *Journal of Molecular Structure*, 1288, 135807. DOI: 10.1016/j.molstruc.2023.135807.

[34] Khan, M.I. (2020). Adsorption of methylene blue onto natural Saudi Red Clay: Isotherms, kinetics and thermodynamic studies. *Materials Research Express*, 7(5), 055507. DOI: 10.1088/2053-1591/ab903c.

[35] Mohammadzadeh, F., Golshan, M., Haddadi-Asl, V., Salami-Kalajahi, M. (2023). Adsorption kinetics of methylene blue from wastewater using pH-sensitive starch-based hydrogels. *Scientific Reports*, 13(1), 1–14. DOI: 10.1038/s41598-023-39241-z.

[36] Sen, T.K. (2023). Adsorptive Removal of Dye (Methylene Blue) Organic Pollutant from Water by Pine Tree Leaf Biomass Adsorbent. *Processes*, 11(7), 1877. DOI: 10.3390/pr11071877.

[37] Kaur, H., Singh, S., Pal, B. (2021). Impact of g-C_3N_4 loading on NiCo LDH for adsorptive removal of anionic and cationic organic pollutants from aqueous solution. *Korean Journal of Chemical Engineering*, 38(6), 1248–1259. DOI: 10.1007/s11814-021-0784-6.

[38] Kheradmand, A., Negarestani, M., Kazemi, S., Shayesteh, H., Javanshir, S., Ghiasinejad, H. (2022). Adsorption behavior of rhamnolipid modified magnetic Co/Al layered double hydroxide for the removal of cationic and anionic dyes. *Scientific Reports*, 12(1), 1–17. DOI: 10.1038/s41598-022-19056-0.

[39] Abdel-Hady, E.E., Mahmoud, R., Hafez, S.H.M., Mohamed, H.F.M. (2022). Hierarchical ternary ZnCoFe layered double hydroxide as efficient adsorbent and catalyst for methanol electrooxidation. *Journal of Materials Research and Technology*, 17, 1922–1941. DOI: 10.1016/j.jmrt.2022.01.042.

[40] Wang, J., Sun, Y., Zhu, B., Wang, T., Wang, Q., Pan, W.P. (2024). Effects of surface functionalizing and pore structure on dissolved mercury adsorption in gasoline by covalent sulphur-doped templated carbons: Experimental and theoretical insights. *Geoenergy Science and Engineering*, 234, 212629. DOI: 10.1016/j.geoen.2023.212629.